Possible New Vortex Matter Phases in $Bi_2Sr_2CaCu_2O_8$

D. T. Fuchs,[1] E. Zeldov,[1] T. Tamegai,[2] S. Ooi,[2] M. Rappaport,[1] and H. Shtrikman[1]
[1]*Department of Condensed Matter Physics, The Weizmann Institute of Science, Rehovot 76100, Israel*
[2]*Department of Applied Physics, The University of Tokyo, Hongo, Bunkyo-ku, Tokyo, 113, Japan*
(Received 12 January 1998)

The vortex matter phase diagram of $Bi_2Sr_2CaCu_2O_8$ crystals is analyzed by investigating vortex penetration through the surface barrier in the presence of a transport current. The strength of the effective surface barrier and its nonlinearity and asymmetry are used to identify a possible new ordered phase above the first-order transition. This technique also allows sensitive determination of the depinning temperature. The solid phase below the first-order transition is apparently subdivided into two phases by a vertical line extending from the multicritical point. [S0031-9007(98)06245-0]

PACS numbers: 74.60.Ge, 74.25.Dw, 74.25.Fy, 74.72.Hs

The traditional view of type II superconductors was that an ordered solid vortex lattice exists over the entire mixed state phase diagram. For high-temperature superconductors, in contrast, it has been suggested theoretically [1,2], and demonstrated experimentally [3–6], that in clean samples the vortex lattice undergoes a first-order melting transition and thus two phases, vortex solid and vortex liquid, are formed. Recent investigations [7–10], however, have shown that the vortex matter phase diagram is comprised of three distinct phases: a rather ordered lattice at low fields, a highly disordered solid at high fields, and a vortex fluid phase at high temperatures. Such a phase diagram is supported by a number of recent theoretical studies [11,12]. In this Letter we show that the phase diagram is even more complex and apparently displays additional new vortex matter phases.

One of the numerous open questions is the structure of the vortex fluid phase, and whether it is further subdivided into two phases: a liquid of vortex lines, and a decoupled gas of vortex pancakes in the CuO planes [13–15]. Both of these fluid phases are weakly pinned, and therefore display high resistivity and reversible magnetization, and thus the existence of a possible transition between them is difficult to resolve. We demonstrate here a new approach for probing such phase transitions. Instead of investigating vortex interaction with the bulk pinning potential, we probe vortex penetration through the surface barrier (SB). It has been shown theoretically that the effective height of the Bean-Livingston SB, and its nonlinear dependence on the driving force, depend on whether the vortices are in a solid, liquid, or gaseous state [16,17]. The recently developed technique [18] for measuring the distribution of the transport current across the sample is well suited for investigation of vortex activation over the SB in the presence of a driving force. It also provides valuable information on the bulk transport properties at low fields and temperatures at which the sample resistivity is below the resolution of conventional transport measurements.

$Bi_2Sr_2CaCu_2O_8$ (BSCCO) crystals ($T_c \simeq 88$ K) were grown using the traveling solvent floating zone method [19]. Silver/gold contacts were evaporated onto freshly cleaved surfaces of single crystals of typical size $150 \times 1500 \times 10\ \mu m^3$. The crystals were positioned on an array of seven Hall sensors that measure the perpendicular component of the magnetic field [5,18] as shown in the inset of Fig. 1. A transport current of 0.5 to 10 mA rms (30–400 Hz) was applied to the crystal. The resulting self-induced ac field B_{ac} was measured by the sensors using a lock-in amplifier [18]. A constant dc magnetic field of 20–5000 G was applied parallel to the c axis. A total of nine crystals was investigated. The characteristic features, which are described below for two typical crystals, were observed in all the samples.

Figure 1(d) shows the self-field B_{ac} vs temperature at a dc field of 1000 G. There are three main forms of transport current flow across the width of the sample, depending on the dynamics of vortices [18], as indicated schematically in Figs. 1(a)–1(c). Figure 1(a): vortices are mobile and their drift velocity is determined by bulk viscosity or pinning. In this case the current flows uniformly across the sample, as it does in a normal metal, and B_{ac} decreases monotonically from one sample edge to the other (Biot-Savart law). Such flow is observed at $T > T_{SB}$ in Fig. 1(d). Figure 1(b): vortices are mobile, but their flow rate across the sample is determined by the low hopping rate over the SB. In this situation most of the current flows at the two edges, where vortices enter and exit the superconductor, in order to provide the necessary driving force to overcome the barrier. Only a very small fraction of the current flows in the bulk to maintain the relatively easy drift of the vortices across the bulk. The resulting self-field distribution inside the sample (sensors 2–7) is opposite both in sign and in slope to that of the uniform flow case. This unusual situation [18] is observed over a wide range $T_d < T < T_{SB}$ in Fig. 1(d). The crossover between the SB and uniform flow occurs gradually between 60–80 K. At the intersection point T_{SB}, half of the current flows in the bulk and half at the two edges of the sample [18]. The dashed line in Fig. 2 shows the field dependence of T_{SB}. Figure 1(c): vortices are immobile for the given applied

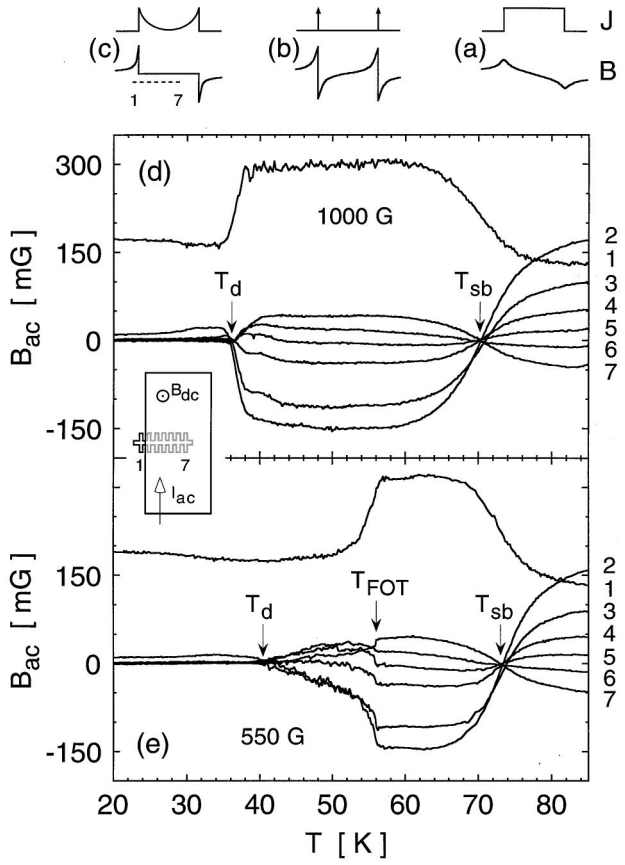

FIG. 1. Schematics of current distribution J, and corresponding self-field B, the transport for (a) uniform current flow, (b) surface barriers, and (c) bulk pinning, with sensor locations indicated. Self-field $B_{\rm ac}$ induced by 4 mA ac current vs T in dc fields of 1000 G (d) and 550 G (e). Curves are labeled by sensor number. Inset: Schematic top view of crystal attached to an array of seven Hall sensors. Sensor 1 is outside the sample and the other six span more than half of the sample width.

current. In this case the transport current distribution has a characteristic Meissner form resulting in $B_{\rm ac} = 0$ within the sample. Such bulk vortex pinning is observed for $T < T_d$. The field dependence of the depinning temperature T_d is shown in Fig. 2.

Figure 1(e) presents similar data at a lower field of 550 G. At fields below 750 G another characteristic temperature is present, $T_{\rm FOT}$, at which the first-order phase transition (FOT) occurs [5]. Above $T_{\rm FOT}$ practically all of the current flows at the edges of the sample. At the transition the relative share of the current in the bulk is suddenly increased, as seen by the drop in the negative self-field signal [linear combination of Fig. 1(b) with a small contribution of 1(a)]. This indicates that the impedance for vortex flow in the bulk is enhanced, as expected for a liquid-solid transition [2]. However, it is important to note that below the transition (i) the vortices are still mobile for all of our applied currents, since $|B_{\rm ac}| > 0$ within the sample, and (ii) the vortex flow rate is still governed by the SB, since $B_{\rm ac}$ profile is inverted (with respect to the uniform flow). Vortices become immobile due to bulk

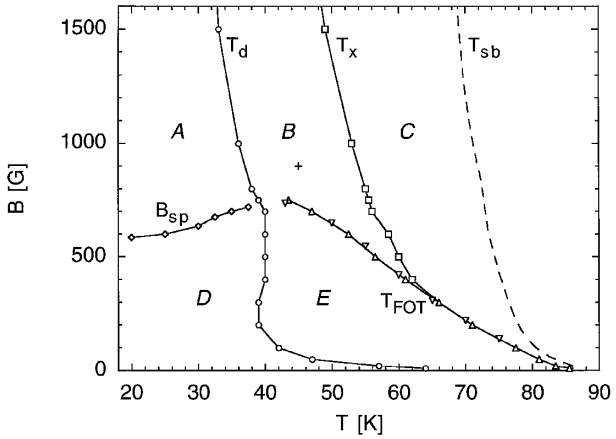

FIG. 2. BSCCO vortex matter phase diagram. Vortices are immobile in phases A and D. Phase B has an intermediate ordered structure between the ordered lattice in phase E and a pancake gas in phase C. The T_x line merges with the $T_{\rm FOT}$ line at low fields. $T_{\rm SB}$ indicates a crossover from uniform to SB dominated current flow.

pinning at the significantly lower temperature T_d. The field dependencies of T_d and $T_{\rm FOT}$ are shown in Fig. 2. The FOT in this crystal was measured independently by detecting the step in the equilibrium magnetization [5] as indicated by the inverted triangles. Figure 2 also shows the position of the second magnetization peak line B_{sp} obtained on the same crystal using local magnetization measurements [7,8]. We emphasize that the observation of the T_d line below B_{sp} is a result of the much higher sensitivity of our technique as compared to the transport measurements for which the resistivity below FOT is immeasurably low.

At the FOT, a sharp drop in sample resistance by typically 2 orders of magnitude is observed [15,20]. This drop is usually ascribed to the onset of pinning upon freezing into the solid phase [3,4]. The data in Fig. 1(e) show that in BSCCO the situation is more complicated; both above and below the FOT vortices are mobile and most of the current flows at the sample edges. The drop in measured resistance therefore reflects a sharp increase in the height of the SB. So upon freezing, both the bulk pinning and the SB increase abruptly, but the vortex flow is still dominated by the hopping rate over the SB.

Above the FOT, bulk pinning is very weak and thus is not efficacious as a probe of the state of the vortex matter. Activation over the SB, on the other hand, is predicted to differ significantly between the possible vortex phases [16,17]. In particular, the effective height of the barrier increases as the order and the c-axis coherence of the vortex matter increase. For a decoupled gas, for example, the pancakes are individually thermally activated over the barrier and the effective barrier height is low [16]. For a liquid of vortex lines, in contrast, a nucleation loop of a minimum critical size has to be created to allow vortex penetration, resulting in a higher effective barrier [16]. In a solid phase, the lattice has to deform

in order to accommodate the penetrating vortex, which further increases the barrier height [17]. Thus, for various processes, the effective barrier height and its nonlinear current dependence are different.

Another important property of the SB is the asymmetry between vortex entry and exit. At equilibrium magnetization, the SB heights for vortex entry and exit are identical [21]. As a result, in the limit of low transport current, the thermally activated transmission through the barrier is linear with the current, and hence the current is equally divided between the two edges of the sample [Fig. 1(b)]. However, due to its asymmetric structure, the barrier height for the vortex exit decreases faster with current than for vortex entry [16,21]. As a result, at high currents the division between the two edges is unequal, with a larger fraction of the current flowing at the vortex entry edge. For an ac transport current, on the positive half cycle, vortices enter at the left edge and exit at the right (see inset of Fig. 1), and vice versa on the negative half cycle. Accordingly, the current on the left edge will be larger on the positive half cycle and smaller on the negative, resulting in a strong second harmonic signal $B_{\rm ac}^{2f}$ [Fig. 3(a)]. This is in sharp contrast to bulk pinning which gives rise only to odd harmonics due to the fact that the bulk I-V characteristics, though nonlinear, are symmetric with respect to the current direction [2]. The local I-V of SB, in contrast, is asymmetric resulting in even harmonics. The asymmetry between the edges grows with the current, and hence for a given barrier strength $B_{\rm ac}^{2f}$ is low at small ac currents and high at large currents. Equivalently, for a given ac current a strong barrier results in a low second harmonic, whereas a weak barrier gives rise to a large $B_{\rm ac}^{2f}$. We use this effect to analyze the activation over the SB as follows. Figure 3(a) shows $B_{\rm ac}^{2f}$ at 10 mA ac current at a 300 and 1000 G dc field. For 300 G a large $B_{\rm ac}^{2f}$ is observed at elevated temperatures indicating a relatively weak SB. At $T_{\rm FOT}$ a discontinuous drop in $B_{\rm ac}^{2f}$ is observed below which the signal vanishes rapidly. For $T_d < T < T_{\rm FOT}$ vortex dynamics is dominated by the SB and most of the current flows on the edges, yet $B_{\rm ac}^{2f}$ is vanishingly small. As discussed above, this shows that the effective SB increases sharply upon freezing. At fields up to $\sim$400 G this SB transition coincides with the FOT. At higher fields, however, we observe a remarkable behavior in which the SB transition follows a new line, labeled T_x in Fig. 2, which resides above the FOT line and extends to elevated fields. Figure 3(a) shows this SB transition at 1000 G. The sharp drop in $B_{\rm ac}^{2f}$ at T_x is very similar to that at $T_{\rm FOT}$ at 300 G. In addition, $B_{\rm ac}^{2f}$ is still finite in the range $T_d < T < T_x$ as compared to vanishing $B_{\rm ac}^{2f}$ at 300 G. This means that the SB in phase B in Fig. 2 has an intermediate value between the strong barrier in phase E and a weak SB in phase C. Indeed, in the field range 400–750 G the SB displays two transitions exemplified below.

An alternative method to investigate the SB is by measuring the first harmonic $B_{\rm ac}$ in the presence of a dc bias current. In the absence of a bias, vortices cross the sample in opposite directions on the positive and negative half cycles of the ac current. Therefore, on average, each edge carries half of the current. Adding a dc bias breaks this symmetry. Figure 3(b) shows an example of $B_{\rm ac}$ at 650 G due to a 4 mA ac current with and without a bias current of ± 6.5 mA, as measured by sensor 3 which is close to the left edge. At $+6.5$ mA bias, vortices enter the sample only from the left. Therefore, at any time, the left barrier is larger than the right one, and thus more than half of the current is flowing on the left edge. As a result a larger $B_{\rm ac}$ (more negative), as compared to zero bias, is measured by sensor 3. For -6.5 mA bias, less than half of the current flows on the left edge and the signal decreases. The degree of splitting between the positive and negative bias curves reflects the strength of the SB. Above T_x the SB is weak and the splitting is large. At T_x the SB is enhanced significantly and the splitting is reduced by about a factor of 2. An additional discontinuous drop in the splitting occurs at $T_{\rm FOT}$ due to a further increase of the SB in the solid phase. At fields below 400 G the two transitions merge into one FOT.

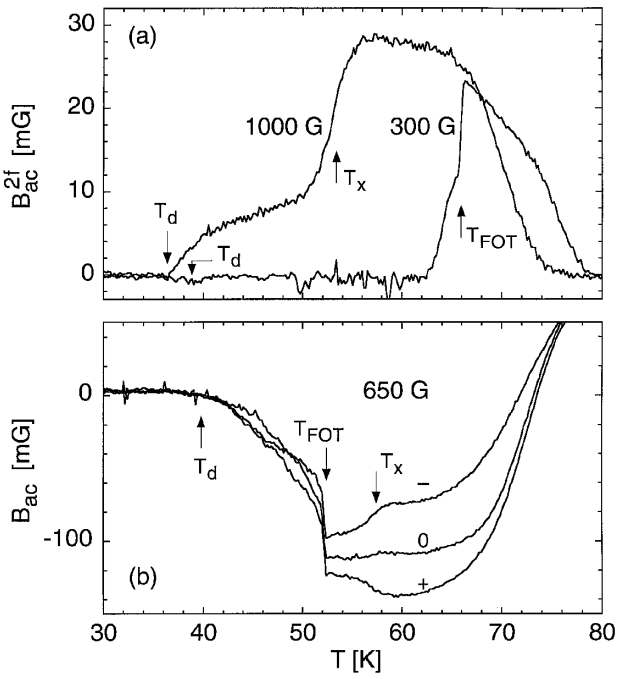

FIG. 3. (a) Second harmonic $B_{\rm ac}^{2f}$ due to SB measured by sensor 3 at 10 mA ac current at 300 and 1000 G. The SB is enhanced abruptly below $T_{\rm FOT}$ and T_x, respectively. (b) First harmonic self-field $B_{\rm ac}$ at 4 mA ac current and 650 G without bias (0) and with positive (+) and negative (−) dc bias of 6.5 mA. The splitting between the + and − curves is reduced at T_x due to enhancement of the SB. An additional drop in the splitting occurs at $T_{\rm FOT}$ due to further enhancement of the SB.

Previous studies of the vortex matter phase diagram in BSCCO have identified three transition lines [7–10] which meet at a multicritical point in Fig. 2: the first-order transition line $T_{\rm FOT}$, the second peak line B_{sp}, and the upper depinning line T_d (above B_{sp}). The corresponding three phases were interpreted as a highly disordered

entangled vortex solid in phase A, one vortex fluid phase in B and C, and phases D and E as one quasilattice or Bragg-glass phase [11,12]. Here we report two additional lines, the T_x line, and the lower T_d line separating the D and E phases (see also Ref. [22]). We find that the vortices are mobile in phase E and immobile in phase D. Therefore one possible explanation is that the lower T_d is depinning within the Bragg-glass phase [11,22]. An interesting observation is that this T_d line drops almost vertically down from the multicritical point, and thus, alternatively, it may reflect a recently suggested phase transition line [23]. Accordingly, phase E is a weakly disordered elastic Bragg glass, whereas phase D is a strongly disordered Josephson glass [23].

We now discuss the T_x line. Recent flux transformer studies [15] suggest that at high temperatures the FOT is a sublimation transition, and hence phase E is a lattice of vortex lines and phase C is a gas of pancakes. Our results here are consistent with this conclusion showing that phase E is the most ordered and coherent one, whereas phase C is highly uncorrelated. The SB behavior suggests the existence of an additional phase B which has a distinct structure with an intermediate degree of order. An important independent insight comes from a recent small angle neutron scattering (SANS) study [24]. The anisotropy of the BSCCO crystal used in these SANS experiments is very similar to ours, resulting in T_{FOT} and B_{sp} lines [9,24,25] which are practically identical to those in Fig. 2. The earlier SANS data [9] indicated that Bragg peaks are present only in the D and E phases. However, a more accurate study demonstrates that the line along which the Bragg peaks disappear follows the FOT line at high temperatures, but then shows an unexpected upturn and continues above the FOT in a "concave" form following our T_x line [24]. Furthermore, at fields above B_{sp} the SANS data show a unique reentrant behavior in which weak but clearly resolvable Bragg peaks are present in the region between T_d and T_x in Fig. 2. For example, Bragg peaks are reported at 900 G and 45 K [24], indicated by a cross in Fig. 2. These results directly support our conclusion that phase B has a structure with intermediate order between that of phases E and C. Another important feature of phase B is gleaned from the study of very low doses of columnar defects [8]. It is found that the vortex matter loses its shear modulus along the T_{FOT} line rather than along the T_x line. Phase B therefore has zero or very low shear modulus.

Since Bragg peaks are observable above the FOT, phase B cannot be an entangled vortex liquid. One possibility is that this phase is a disentangled liquid of lines, as was proposed for $YBa_2Cu_3O_7$ [14], with some sort of hexatic order that results in weak Bragg peaks. Another possibility is the supersolid [26,27], decoupled solid [13,23], or soft solid [28] phase, which consists of a rather well aligned stack of ordered 2D pancake layers. Such a phase is predicted to have a very low shear modulus due to vortex vacancies or interstitials, and is expected to display Bragg peaks. This interesting scenario implies that the T_{FOT} is a first-order decoupling [13,23,29] or softening [28] transition rather than melting, T_x is melting of the supersolid, and B_{sp} is a disorder induced decoupling [23] rather than a disorder induced solid entanglement [11,12]. Finally, as will be described elsewhere, the T_d line displays some current and frequency dependence, whereas the T_{FOT} and T_x lines do not. It therefore remains to be determined which of the lines in Fig. 2 reflect thermodynamic phase transitions.

We thank V. Geshkenbein, A. Stern, B. Horovitz, M. Konczykowski, and R. Doyle for valuable discussions. This work was supported by the Israel Ministry of Science and the Grant-in-Aid for Scientific Research from the Ministry of Education, Science, Sports and Culture, Japan, by the Israel Science Foundation, and by the MINERVA Foundation, Munich, Germany.

[1] D. R. Nelson, Phys. Rev. Lett. **60**, 1973 (1988).
[2] G. Blatter *et al.*, Rev. Mod. Phys. **66**, 1125 (1994); E. H. Brandt, Rep. Prog. Phys. **58**, 1465 (1995).
[3] H. Safar *et al.*, Phys. Rev. Lett. **69**, 824 (1992).
[4] W. K. Kwok *et al.*, Phys. Rev. Lett. **69**, 3370 (1992).
[5] E. Zeldov *et al.*, Nature (London) **375**, 373 (1995).
[6] A. Schilling *et al.*, Nature (London) **382**, 791 (1996).
[7] B. Khaykovich *et al.*, Phys. Rev. Lett. **76**, 2555 (1996).
[8] B. Khaykovich *et al.*, Phys. Rev. B **56**, R517 (1997).
[9] R. Cubitt *et al.*, Nature (London) **365**, 407 (1993).
[10] S. L. Lee *et al.*, Phys. Rev. Lett. **71**, 3862 (1993).
[11] D. Ertas and D. R. Nelson, Physica (Amsterdam) **272C**, 79 (1996).
[12] T. Giamarchi and P. Le Doussal, Phys. Rev. B **55**, 6577 (1997); V. M. Vinokur *et al.*, Physica (Amsterdam) **C** (to be published).
[13] L. Glazman and A. Koshelev, Phys. Rev. B **43**, 2835 (1991); L. Daemen *et al.*, Phys. Rev. B **47**, 11 291 (1993).
[14] A. V. Samoilov *et al.*, Phys. Rev. Lett. **76**, 2798 (1996).
[15] D. T. Fuchs *et al.*, Phys. Rev. B **55**, R6156 (1997).
[16] L. Burlachkov, A. E. Koshelev, and V. M. Vinokur, Phys. Rev. B **54**, 6750 (1996).
[17] A. E. Koshelev, Physica (Amsterdam) **223C**, 276 (1994).
[18] D. T. Fuchs *et al.*, Nature (London) **391**, 373 (1998).
[19] N. Motohira *et al.*, J. Ceram. Soc. Jpn. **97**, 994 (1989).
[20] D. T. Fuchs *et al.*, Phys. Rev. B **54**, 796 (1996); S. Watauchi *et al.*, Physica (Amsterdam) **259C**, 373 (1996).
[21] J. R. Clem, *Low Temperature Physics-LT 13*, edited by K. D. Timmerhaus *et al.* (Plenum, New York, 1974), Vol. 3, p. 102.
[22] C. D. Dewhurst and R. A. Doyle, Phys. Rev. B **56**, 10 832 (1997).
[23] B. Horovitz and T. R. Goldin, Phys. Rev. Lett. **80**, 1734 (1998).
[24] E. M. Forgan *et al.*, Czech. J. Phys. **46**, 1571 (1996).
[25] P. H. Kes, *et al.*, J. Phys. I (France) **6**, 2327 (1996).
[26] E. Frey, D. R. Nelson, and D. S. Fisher, Phys. Rev. B **49**, 9723 (1994).
[27] M. V. Feigel'man, V. B. Geshkenbein, and A. I. Larkin, Physica (Amsterdam) **167C**, 177 (1990).
[28] H. M. Carruzzo and C. C. Yu, Philos. Mag. B **77**, 1001 (1998).
[29] R. A. Doyle *et al.*, Phys. Rev. Lett. **75**, 4520 (1995).